Human Molecular Genetics, 2012, Vol. 21, No. 21 **4587–4601**
doi:10.1093/hmg/dds297
Advance Access published on July 27, 2012

Enhanced β-secretase processing alters APP axonal transport and leads to axonal defects

Elizabeth M. Rodrigues[1], April M. Weissmiller[2,3] and Lawrence S.B. Goldstein[2,3,4,*]

[1]Division of Biological Sciences, [2]Department of Cellular and Molecular Medicine, [3]Department of Neurosciences and [4]Howard Hughes Medical Institute, University of California, San Diego, 9500 Gilman Dr., La Jolla, California 92093, USA

Received April 19, 2012; Revised July 5, 2012; Accepted July 17, 2012

Alzheimer's disease (AD) is a neurodegenerative disease pathologically characterized by amyloid plaques and neurofibrillary tangles in the brain. Before these hallmark features appear, signs of axonal transport defects develop, though the initiating events are not clear. Enhanced amyloidogenic processing of amyloid precursor protein (APP) plays an integral role in AD pathogenesis, and previous work suggests that both the Aβ region and the C-terminal fragments (CTFs) of APP can cause transport defects. However, it remains unknown if APP processing affects the axonal transport of APP itself, and whether increased APP processing is sufficient to promote axonal dystrophy. We tested the hypothesis that β-secretase cleavage site mutations of APP alter APP axonal transport directly. We found that the enhanced β-secretase cleavage reduces the anterograde axonal transport of APP, while inhibited β-cleavage stimulates APP anterograde axonal transport. Transport behavior of APP after treatment with β- or γ-secretase inhibitors suggests that the amount of β-secretase cleaved CTFs (βCTFs) of APP underlies these transport differences. Consistent with these findings, βCTFs have reduced anterograde axonal transport compared with full-length, wild-type APP. Finally, a gene-targeted mouse with familial AD (FAD) Swedish mutations to APP, which enhance the β-cleavage of APP, develops axonal dystrophy in the absence of mutant protein overexpression, amyloid plaque deposition and synaptic degradation. These results suggest that the enhanced β-secretase processing of APP can directly impair the anterograde axonal transport of APP and are sufficient to lead to axonal defects *in vivo*.

INTRODUCTION

Amyloid precursor protein (APP) plays an essential role in the pathogenesis of Alzheimer's disease (AD), a prevalent neurodegenerative disease in which patients suffer cognitive decline and memory loss. Pathological hallmarks of AD brains include intracellular neurofibrillary tangles and extracellular amyloid plaques. A primary component of amyloid plaques is Aβ, a peptide derived from the sequential proteolytic processing of APP by β- and γ-secretases. APP is a transmembrane protein that undergoes axonal transport (1–5), but it is not clear how proteolytic processing of APP affects its axonal transport properties. It is known that full-length APP and its C-terminal fragments (CTFs) accumulate at terminal fields (6) following anterograde axonal transport and may undergo further processing into Aβ that is released at the synapse (7). Full-length APP and cleavage fragments are reported to localize into distinct neuritic vesicles (8,9); however, there is no precise comparative characterization of their individual transport behaviors.

Elucidating the influence that proteolytic processing has on APP axonal transport may provide important insight into understanding the phenotypes characteristic of axonal transport defects that develop both early and late in AD. Before the hallmark pathologies of amyloid plaques and neurofibrillary tangles develop, axonal swellings can be found in sporadic AD brains (10). These types of axonal swellings, consisting of accumulated organelles and vesicles, have previously been described in animal models with mutations in genes encoding motor protein components, as well as in animal models that overexpress wild-type (WT) or familial AD (FAD) mutant APP (2,10–16).

Transgenic mice overexpressing FAD Swedish APP mutations (Tg-swAPP^{Prp}) develop the phenotypes typical of

*To whom correspondence should be addressed at: University of California, San Diego, 9500 Gilman Drive #0695, La Jolla, CA 92093-0695, USA. Tel: +1 8585349702; Fax: +1 8582461579; Email: lgoldstein@ucsd.edu

axonal transport defects similar to those seen in sporadic AD (10). Swedish mutations of APP enhance the β-secretase cleavage of APP and are sufficient to cause FAD (17). Intriguingly, β-secretase cleaved CTFs (βCTFs) generated from the β-secretase cleavage of APP are also found to be increased in sporadic AD brains (18), as are protein levels and the enzymatic activity of the APP β-secretase (BACE) (19,20). A previous study has shown that elevated βCTF levels induce endosomal defects (21), which is also an early feature of sporadic AD (22). These findings highlight the importance of investigating the β-secretase cleavage of APP in disease mechanisms, and as a potential regulator of APP axonal transport. Other perturbations to APP, such as overexpression and deletion, have also been found to disrupt axonal transport, with overexpression phenotypes dependent on the APP C terminus (2,14,23–25). In addition to the finding that axonal transport defects can be caused by the overexpression of the APP C terminus (2), Aβ is reported to cause axonal transport defects when added exogenously (26–32). Since the β-secretase cleavage of APP generates βCTFs that are subsequently cleaved by γ-secretases to generate Aβ, it is possible that the enhanced β- or γ-secretase cleavage of APP could affect the axonal transport of APP specifically. However, the relative contributions to axonal transport defects of APP processing to βCTF or Aβ, or of APP overexpression, are unknown and have not been directly studied.

Here, we tested the hypotheses that the enhanced β-secretase cleavage of APP directly alters APP axonal transport in cultured mouse hippocampal neurons and is sufficient to lead to axonal defects *in vivo* without overexpression. We performed a detailed characterization of the live axonal transport of full-length APP, full-length APP mutated at its β-secretase cleavage site and C-terminal APP cleavage products, in order to compare their axonal transport behaviors. Direct examination of WT and mutant APP real-time axonal transport demonstrated that enhanced β-secretase cleavage reduces APP anterograde axonal transport, while inhibited β-secretase cleavage stimulates it. Our analyses specifically implicated βCTF production, rather than αCTF or Aβ production, for these differences in axonal transport behaviors. βCTFs also showed decreased anterograde axonal transport compared with full-length APP. To clarify if the overexpression of mutant APP is necessary to induce axonal defects, we examined a gene-targeted mouse. Analysis revealed that FAD Swedish mutations of APP, which enhance β-secretase cleavage, are sufficient to induce plaque-independent axonal dystrophy in the form of axonal dilation, even when mutant APP is expressed at endogenous levels. Axonal defects occurred in the absence of any detectable synaptic degradation. These results suggest that the enhanced β-secretase processing of APP can reduce the anterograde axonal transport of APP itself and can contribute to the development of axonal defects *in vivo*.

RESULTS

APP-YFP β-secretase cleavage site mutations alter its cleavage

To test if alterations in the β-secretase cleavage of APP can affect APP axonal transport properties, we generated and characterized two mutant forms of human APP tagged with yellow fluorescent protein (APP-YFP). FAD Swedish APP-YFP possesses two mutations at the β-secretase cleavage site (K595N and M596L) to enhance β-secretase cleavage (17,33). M596V APP-YFP has a single mutation at the same site to inhibit β-secretase cleavage (34) (Fig. 1B). To confirm that Swedish and M596V mutant APP-YFP undergo enhanced or suppressed β-secretase cleavage, respectively, we performed western blots from cells transfected with WT, FAD Swedish (**SWE**) or M596V (**MV**) APP-YFP. The C-terminal β-secretase cleavage product of APP-YFP, βCTF-YFP, was increased in cells transfected with SWE APP-YFP and decreased in cells transfected with MV APP-YFP compared with WT APP-YFP (Fig. 1C). Levels of full-length, endogenous mouse APP remained relatively unchanged. Thus, as expected, mutations of the β-secretase cleavage site of APP-YFP alter its cleavage by β-secretase.

FAD Swedish mutations reduce the anterograde axonal transport of APP-YFP

Although the overexpression of FAD Swedish APP causes axonal transport phenotypes in *Drosophila* and mouse (2,10), the effects of these mutations specifically on APP vesicle movement dynamics in axons remain untested. In order to understand the role that proteolytic processing plays in APP axonal transport, we first compared the axonal transport dynamics of SWE APP-YFP to those of WT APP-YFP.

Primary cultures of mature hippocampal neurons with well-established axonal projections from WT mice were transfected at 10 days *in vitro* with either WT or SWE APP-YFP. Experiments were carefully designed so data could be collected in parallel, and only data from multiple repetitions of these experiments performed on several different days were compared with each other. In addition, several culture preparations were transfected, and several different plasmid preparations of each construct were used. Care was taken to collect data only from axons of neurons lacking any gross morphological signs of cellular toxicity. A large amount of fluorescent protein was present within transfected cell bodies (Fig. 2A), but individual puncta of moving APP-YFP-containing vesicles were visible within axons distal to the cell body (Fig. 2B, arrows). Neurons transfected with WT or SWE APP-YFP showed similar numbers (Fig. 2C) and intensities (Fig. 2D) of fluorescent particles in axons, suggesting that there is no major difference in the amount of tagged protein that enters axons under these conditions.

Movement of APP-YFP vesicles across time was plotted on kymographs (Fig. 2E) and analyzed. FAD Swedish mutations induced obvious changes to the axonal transport of APP-YFP vesicles, including a significant decrease in the percentage of SWE APP-YFP particles moving in the anterograde direction when compared with WT APP-YFP (Fig. 2F; $P = 0.017$). More precise characteristics of axonal transport dynamics include segmental velocity and run length, which are defined as the speed and distance a particle travels in one direction without being interrupted by a pause in movement or a reversal in direction traveling. Segmental velocities and run lengths of anterograde and retrograde SWE APP-YFP were comparable with WT (Fig. 2G and H). Thus, FAD Swedish mutations, which enhance the β-secretase cleavage of APP, alter axonal transport of APP itself by reducing its anterograde transport.

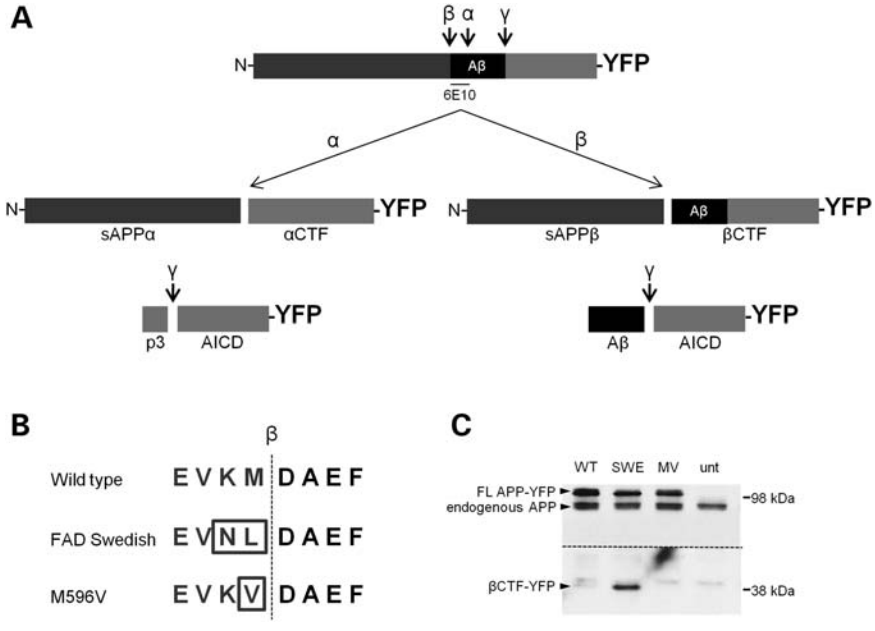

Figure 1. APP-YFP β-secretase cleavage site mutations alter its cleavage. (**A**) A schematic representation of the APP protein tagged with YFP, with the secretase cleavage sites indicated. Aβ region is indicated in black, and the 6E10 antibody epitope is identified. Cleavage products formed upon α-, β- and γ-secretase cleavage are indicated. (**B**) Amino acid sequence flanking the β-secretase cleavage site (indicated by dotted line) for WT, SWE and MV APP-YFP. (**C**) Western blot of SH-SY5Y cells transfected with WT and mutant (SWE and MV) APP-YFP and untransfected (unt) cells as a control. The 6E10 antibody epitope lies in the Aβ region, so it will recognize full-length APP-YFP and βCTF-YFP, but not the αCTF-YFP. Top arrowheads identify full-length APP-YFP and full-length endogenous APP bands, and bottom arrowhead identifies βCTF-YFP bands. Both YFP bands are absent in the untransfected control. Above the dotted line is the membrane at a low exposure. Below the dotted line is the same membrane at a higher exposure to reveal the βCTF-YFP bands. This higher exposure also reveals a set of non-specific bands present in all samples that lies immediately above the βCTF-YFP bands.

Inhibition of β-secretase cleavage by the MV mutation enhances the anterograde axonal transport of APP

Because FAD Swedish mutations at the β-secretase cleavage site of APP enhance its cleavage by β-secretase and reduce APP anterograde axonal transport, we tested the ability of β-secretase cleavage inhibition to stimulate anterograde APP axonal transport. Thus, we examined the axonal transport of APP-YFP with an M596V mutation at the β-secretase cleavage site, which inhibits the β-secretase cleavage of APP (34) (Fig. 1C). Mouse hippocampal neurons transfected with MV APP-YFP had similar numbers and intensities (Fig. 3A and B) of fluorescent particles in axons as neurons transfected with WT APP-YFP, suggesting that there is no major difference in the amount of tagged protein that enters axons.

The MV mutation stimulated the anterograde axonal transport of APP-YFP (Fig. 3C), including a significant increase in the percentage of particles moving in the anterograde direction ($P = 0.007$) and a decrease in the retrograde direction ($P = 0.045$) compared with WT APP-YFP (Fig. 3D). Anterograde, but not retrograde, segmental velocity ($P = 0.026$) and run length ($P = 0.003$) of MV APP-YFP significantly increased compared with WT (Fig. 3E and F). Strikingly, SWE and MV mutations have opposite effects on the β-secretase cleavage of APP and opposite effects on APP axonal transport, suggesting that the β-secretase cleavage of APP can contribute to the regulation of APP axonal transport properties.

Pharmacological inhibition of β-secretase stimulates APP anterograde axonal transport, but γ-secretase inhibition reduces it

Given that mutations to the β-secretase cleavage site of APP alter APP axonal transport, we further tested the ability of β-secretase cleavage to regulate APP axonal transport by using a non-genetic approach. Specifically, since FAD Swedish mutations enhance the β-secretase cleavage of APP, a key prediction is that the pharmacological inhibition of β-secretase should suppress the reduced anterograde axonal transport phenotype of FAD Swedish APP-YFP. We found that 40 μM β-secretase inhibitor significantly increased the percentage of FAD Swedish APP-YFP particles moving in the anterograde direction ($P = 0.006$) and decreased the percentage of retrograde particles ($P = 0.019$) compared with FAD Swedish APP-YFP with vehicle alone (Fig. 4A). Neurons treated with the drug did not show any gross signs of cellular toxicity (data not shown), and a lower 10 μM dose had a reduced effect on transport (Fig. 4A). These results in which impaired anterograde axonal transport of SWE APP-YFP can be reversed with β-secretase inhibition suggest that the FAD Swedish APP transport phenotype is likely due to enhanced β-secretase cleavage caused by the mutations.

Although a β-secretase inhibitor was able to reverse the effects of FAD Swedish mutations on APP axonal transport, it will inhibit the cleavage of both transfected APP-YFP and endogenous APP. We set out to distinguish which is

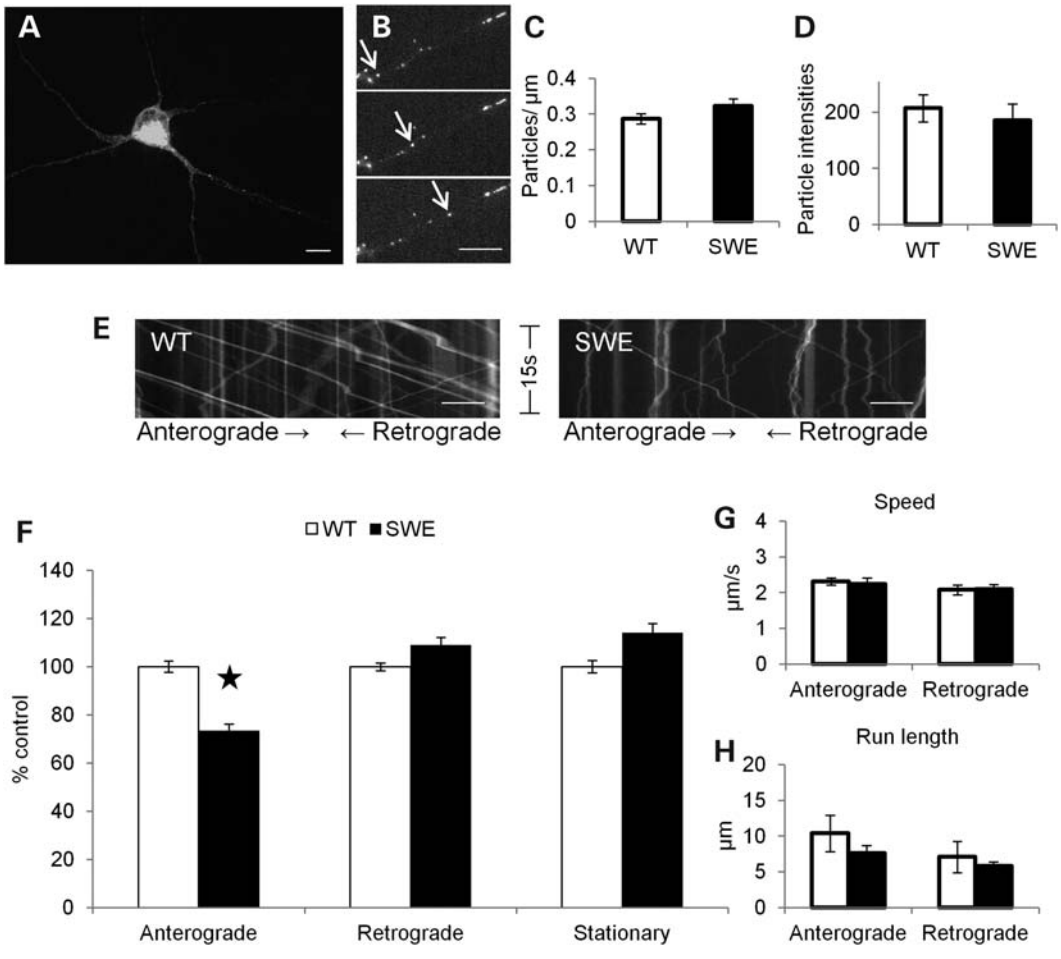

Figure 2. FAD Swedish mutations reduce APP anterograde axonal transport. (**A**) Confocal image of a mouse hippocampal neuron transfected with SWE APP-YFP. Scale bar = 10 μm (**B**) Fluorescent SWE APP-YFP particles in an axon. Arrows follow a single particle traveling in the anterograde direction across chronological frames (top to bottom) from a movie used in data analysis. Scale bar = 10 μm. (**C**–**H**) WT APP-YFP (white) $n = 40$ axons, 1009 particles and SWE APP-YFP (black) $n = 40$ axons, 1129 particles. (C) The mean number of fluorescent particles per length of transfected mouse hippocampal axon. (D) The mean fluorescent intensities of axonal particles. (E) Representative kymographs for WT and FAD Swedish APP-YFP axonal transport from 15s, 10 Hz movies. Right or left descending particles represent anterograde or retrograde moving vesicles, respectively. Vertical lines represent stationary particles. (F) Percentage of anterograde ($P = 0.017$), retrograde and stationary SWE APP-YFP particles compared with WT. Average segmental velocities (G) and segmental run lengths (H) for anterograde and retrograde APP-YFP particles obtained from kymograph analyses. (Student's *t*-tests, $^{*}P < 0.05$.

responsible for altering SWE APP-YFP axonal transport. If the inhibitor alters SWE APP-YFP axonal transport by acting directly on SWE APP-YFP, then the inhibitor treatment of MV APP-YFP would be predicted to have no effect on MV APP-YFP axonal transport, since it already has inhibited β-secretase cleavage as a result of the M596V mutation. We found that MV APP-YFP treated with 40 μM β-secretase inhibitor showed normal axonal transport that was comparable with MV APP-YFP with vehicle alone (Fig. 4B). 40 μM β-secretase inhibitor dramatically increased FAD Swedish APP anterograde axonal transport, but had no effect on MV APP axonal transport, indicating a direct role for βCTF production on APP axonal transport instead of an indirect or toxic effect of the inhibitor. In addition, these results suggest that the stimulation of APP anterograde axonal transport caused by the MV mutation is likely due to its inhibited β-cleavage of APP-YFP.

Typically, the β-secretase cleavage of APP is followed by γ-secretase cleavage to generate Aβ, the primary component of amyloid plaques. Some studies report that Aβ can induce general axonal transport defects in cell culture (26–32,35,36), but evidence from transgenic mice and *Drosophila* suggests that Aβ is not the only fragment of APP that causes axonal transport defects that result from perturbations to APP *in vivo* (2,24,37). To investigate the role that Aβ plays in altered APP transport upon increased βCTF generation, a γ-secretase inhibitor was used with SWE APP-YFP to reduce Aβ production and raise βCTF-YFP levels. Pharmacological inhibition with 5 μM, but not a lower dose of 100 nM, γ-secretase inhibitor further reduced SWE APP-YFP anterograde axonal transport, by decreasing the percentage of anterograde ($P = 0.002$) and increasing the percentage of retrograde ($P = 0.001$) axonal transport compared with SWE APP-YFP with vehicle alone (Fig. 4C). Neurons treated with this drug did not show any signs of cellular

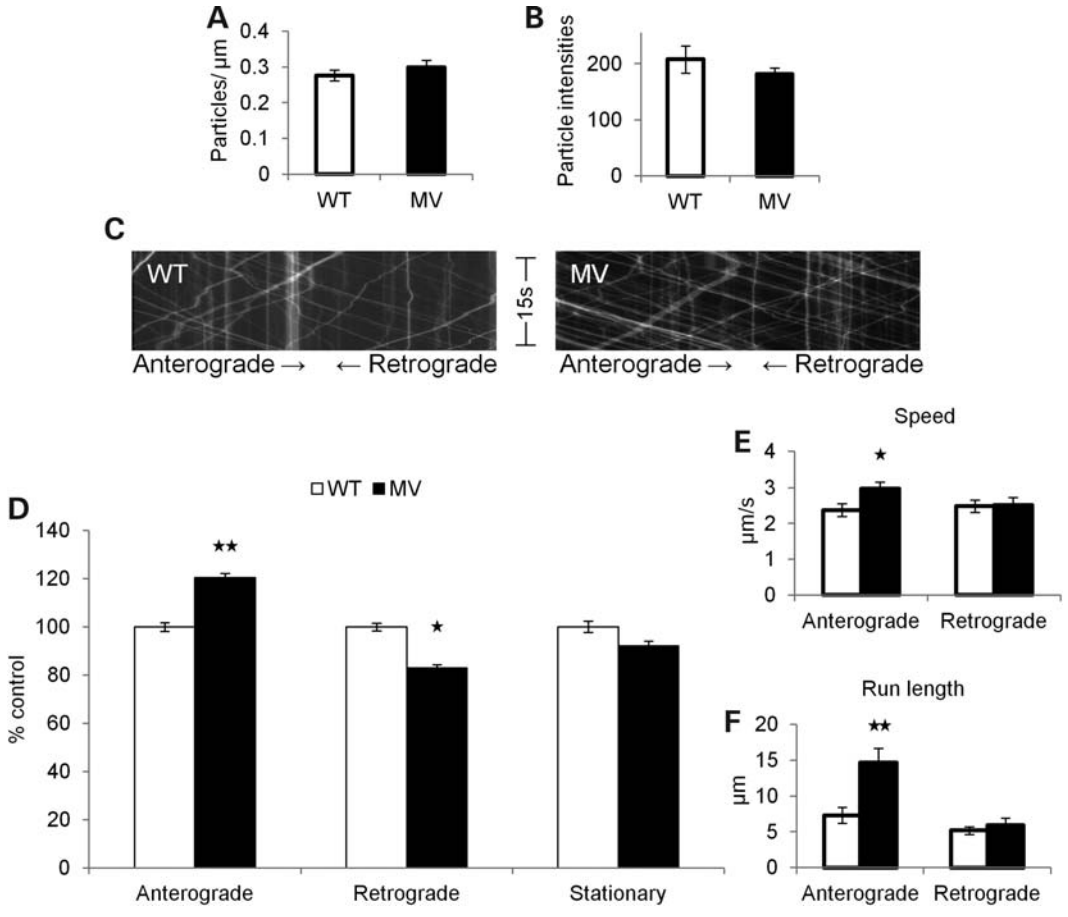

Figure 3. MV mutation stimulates APP anterograde axonal transport. (**A**–**F**) WT APP-YFP (white) $n = 44$ axons, 1172 particles, and MV APP-YFP (black) $n = 52$ axons, 1577 particles. (A) The mean number of fluorescent particles per length of transfected mouse hippocampal axon. (B) The mean fluorescent intensities of axonal particles. (C) Representative kymographs for WT and MV APP-YFP axonal transport. (D) Percentage of anterograde ($P = 0.007$), retrograde ($P = 0.045$) and stationary MV APP-YFP particles compared with WT. Average segmental velocities (E) and segmental run lengths (F) for anterograde ($P = 0.026$ and $P = 0.003$, respectively) and retrograde APP-YFP particles obtained from kymograph analyses (Student's *t*-tests, $^{*}P < 0.05$, $^{**}P < 0.01$).

toxicity (data not shown). The ability of the γ-secretase inhibitor to alter APP axonal transport in an opposing manner to the β-secretase inhibitor argues for specificity of these inhibitors and against indirect drug toxicity effects. Thus, reducing Aβ production and increasing βCTF-YFP levels exacerbated the decreased anterograde axonal transport phenotype of SWE APP-YFP. These data suggest that enhanced β-secretase cleavage by FAD Swedish mutations is sufficient to impair anterograde APP axonal transport by a mechanism that is likely βCTF-dependent and Aβ-independent.

APP βCTFs exhibit impaired anterograde axonal transport

Since our data suggest that the enhanced β-secretase cleavage of APP impairs APP anterograde axonal transport, while inhibited β-secretase cleavage stimulates it, it implies that these phenotypes simply result from alterations in βCTF levels. However, our experiments described so far inherently do not distinguish full-length APP-YFP from CTF-YFP axonal transport. To test the hypothesis that βCTFs have reduced anterograde axonal transport compared with full-length APP, we examined the axonal transport of CTFs tagged with enhanced green fluorescent protein (EGFP).

We transfected neurons with βCTF-EGFP and compared its axonal transport with that of WT APP-EGFP. Cells transfected with βCTF-EGFP do not express any full-length APP-EGFP (Fig. 5A). Mouse hippocampal neurons transfected with either full-length WT APP-EGFP or βCTF-EGFP showed similar numbers of fluorescent particles in axons, suggesting that there is no major difference in the amount of tagged protein that enters axons (Fig. 5B). However, βCTF-EGFP exhibited severely reduced anterograde axonal transport compared with WT APP-EGFP (Fig. 5C), including a significantly decreased percentage of anterograde ($P < 0.001$) and an increased percentage of retrograde ($P = 0.003$) axonal transport, along with an increase in the percentage of stationary particles ($P = 0.024$; Fig. 5D). Both anterograde segmental velocity ($P = 0.001$) and run length ($P < 0.001$) significantly decreased compared with WT APP-EGFP, while retrograde segmental velocity increased ($P = 0.025$; Fig. 5E and F). Thus, βCTF-EGFP exhibits reduced anterograde axonal transport compared with WT APP-EGFP, with a phenotype much more drastic than the SWE APP-YFP phenotype. These data

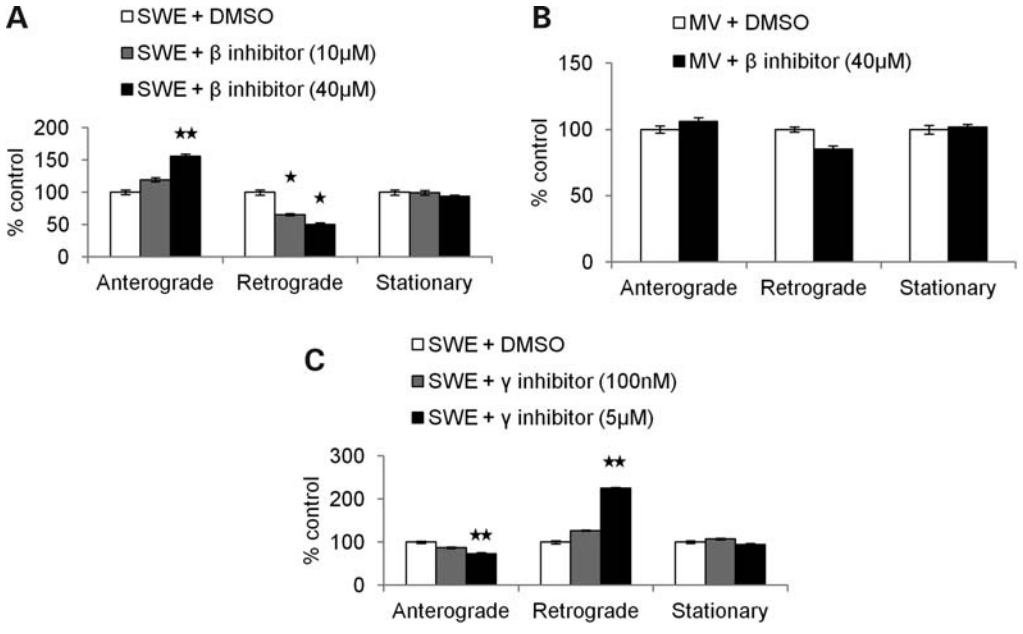

Figure 4. Pharmacological inhibition of β- and γ-secretase activity alters APP axonal transport. (**A**) Percentage of anterograde, retrograde and stationary SWE APP-YFP particles treated with 10 μM β-secretase inhibitor (gray, $n = 25$ axons, 598 particles) or 40 μM β-secretase inhibitor (black, $n = 22$ axons, 445 particles) compared with DMSO (white, $n = 25$ axons and 697 particles for 10 μM data set, $n = 18$ axons and 234 particles for 40 μM data set). Anterograde axonal transport significantly increased with 40 μM β-secretase inhibitor ($P = 0.006$), while retrograde transport decreased with both 10 and 40 μM inhibitor ($P = 0.018$ and $P = 0.019$, respectively). (**B**) Percentage of anterograde, retrograde and stationary MV APP-YFP particles treated with 40 μM β-secretase inhibitor (black, $n = 33$ axons, 309 particles) compared with DMSO (white, $n = 29$ axons, 373 particles). (**C**) Percentage of anterograde ($P = 0.002$), retrograde ($P = 0.001$) and stationary SWE APP-YFP particles treated with 100 nM ($n = 49$ axons, 1499 particles) or 5 μM γ-secretase inhibitor (black, $n = 22$ axons, 674 particles) compared with DMSO (white, $n = 35$ axons and 995 particles for 100 nM data set, $n = 12$ axons and 322 particles for 5 μM data set) (Student's t tests, $^{*}P < 0.05$, $^{**}P < 0.01$).

support the hypothesis that the altered axonal transport of FAD Swedish APP is due to an increased proportion of βCTFs and demonstrate directly divergent live axonal transport behavior of full-length APP and βCTFs.

Inhibiting the β-secretase cleavage of APP by the M596V mutation enhances its anterograde axonal transport, but this could possibly be due to an increased proportion of either full-length APP or αCTFs. To address this issue, we transfected neurons with αCTF-EGFP to compare its axonal transport with WT APP-EGFP. Western blots of transfected cells showed the presence of the αCTF-EGFP product when probed with a C-terminal APP antibody (Fig. 5G). However, neurons transfected with αCTF-EGFP only exhibited diffuse fluorescence in neurites. Therefore, the axonal transport of punctate particles was not observed (Fig. 5H), as with APP-EGFP and βCTF-EGFP.

Axonal defects in an FAD Swedish APP gene-targeted mouse

Taken together, our *in vitro* results indicate a direct impact of APP processing on axonal transport properties of APP vesicles, such that FAD Swedish mutations that enhance the β-secretase cleavage of APP inhibit its anterograde axonal transport. Flies and mice overexpressing FAD Swedish APP also develop phenotypes typical of axonal transport defects (2,10). Enhanced β-secretase processing is thought to occur in both sporadic and FAD (17–20,33), and AD brains characteristically display axonal dystrophy (38–42). APP is not overexpressed, however, in sporadic or FAD, as it is in these FAD Swedish APP animal models previously studied. It remains unanswered whether FAD Swedish mutations enhancing the β-secretase cleavage of APP are sufficient to cause axonal defects, or if the overexpression of the mutant protein is required as well.

To address this issue, we tested the hypothesis that FAD Swedish mutations could lead to axonal defects in a mouse model that does not overexpress APP. We examined axonal phenotypes of neurons in a gene-targeted mouse that has FAD Swedish mutations and a humanized Aβ region targeted to the mouse APP gene (Fig. 5A). Previous studies report increased β-secretase cleavage and Aβ generation without amyloid plaque deposition (43,44), emphasizing the use of this mouse as a model of the earliest changes that might occur in the disease process.

We assessed axonal morphologies in the cholinergic basal forebrain, a location known to show axonal transport defects in AD brains and Tg-swAPP^{Prp} mice (10). Immunohistochemistry for choline acetyltransferase (ChAT), the enzyme that catalyzes the final step in acetylcholine biosynthesis, was performed to identify cholinergic axonal morphology in the septal nucleus. A significant increase in dilated axons over 1.5 μm in diameter was observed in the septohippocampal region of the septal nucleus of 12-month-old gene-targeted mice compared with WT, age-matched littermates (Fig. 6B), including both the total length and number of dilated axons (Fig. 6C and D, $\alpha < 0.05$). This phenotype was specific to the septohippocampal subregion of the septal nucleus and was not observed in the

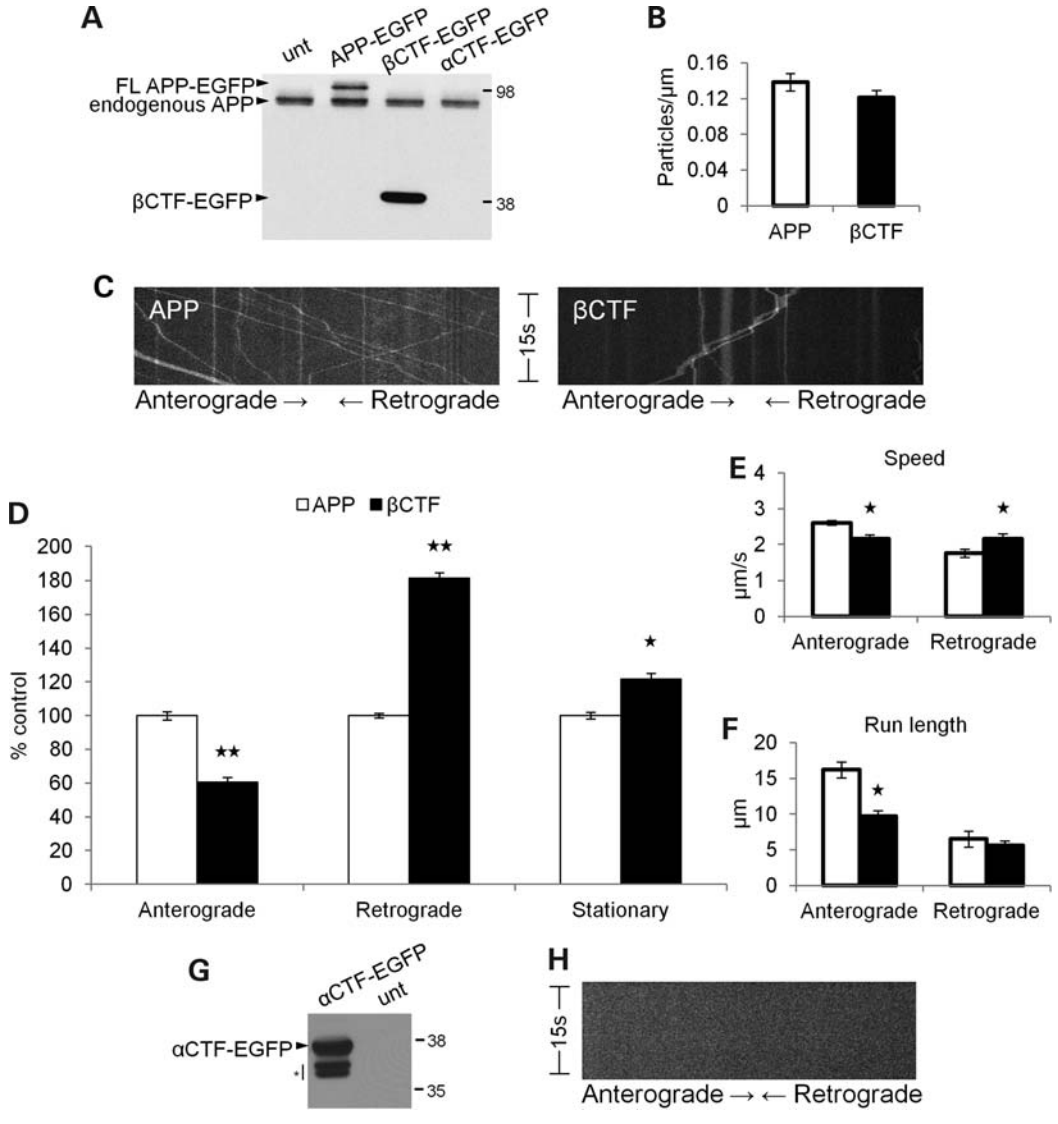

Figure 5. βCTFs have reduced anterograde axonal transport. (**A**) Western blot of SH-SY5Y cells transfected with WT APP-EGFP, βCTF-EGFP, αCTF-EGFP and untransfected (unt) cells as a control. The 6E10 antibody epitope lies in the Aβ region, so it will recognize full-length APP-EGFP and βCTF-EGFP, but not αCTF-EGFP. Top arrowhead identifies the full-length APP-EGFP band present only in APP-EGFP transfected cells, and bottom arrowhead identifies the βCTF-EGFP band that is absent in αCTF-EGFP transfected cells. (**B**–**F**) WT APP-EGFP (white) $n = 52$ axons, 658 particles, βCTF-EGFP (black) $n = 38$ axons, 448 particles. (B) The mean number of fluorescent particles per length of transfected mouse hippocampal axon. (C) Representative kymographs for WT APP-EGFP and βCTF-EGFP axonal transport. (D) Percentage of anterograde ($P < 0.001$), retrograde ($P = 0.003$) and stationary ($P = 0.024$) particles for βCTF-EGFP compared with WT APP-EGFP. Segmental velocities (E) and run lengths (F) for anterograde ($P = 0.001$ and $P < 0.001$, respectively) and retrograde ($P = 0.025$) particles obtained from kymograph analyses. (G) Western blot of cells transfected with αCTF-EGFP and the untransfected control, probed with a C-terminal APP antibody. Below αCTF-EGFP product lies two bands of unidentified/degradation products (indicated by asterisk), which were previously reported with the βCTF-EGFP plasmid from which this αCTF-EGFP plasmid was constructed (85). (H) Representative kymograph for αCTF-EGFP showing no axonal transport (Student's *t*-tests, $^{*}P < 0.05$, $^{**}P < 0.01$).

medial or intermediate septal subregions (Fig. 6C and D). Thus, FAD Swedish mutations to APP that we have shown alter axonal transport of APP *in vitro* can also lead to axonal defects *in vivo*, even when mutant APP is not overexpressed.

We demonstrated *in vitro* that the β-secretase processing of APP can alter its axonal transport, which could potentially also affect the delivery of necessary components to axon terminals. Because FAD Swedish APP gene-targeted mice develop axonal changes, we tested if synapses in their corresponding terminal field were also affected. Therefore, we tested for decreased innervation of septal nucleus terminal fields in the hippocampus. Immunohistochemistry was performed for both ChAT and the presynaptic marker synaptophysin, and density of labeling was measured in the hippocampus. FAD Swedish APP gene-targeted mice show comparable levels of synaptic density to WT mice through the age of 24 months, using both ChAT (Fig. 6E) and synaptophysin (Fig. 6F–I) as probes. Cholinergic axonal dilation in gene-targeted mice does not correlate with decreased presynaptic density in corresponding terminal fields. Thus, the axonal defect observed in

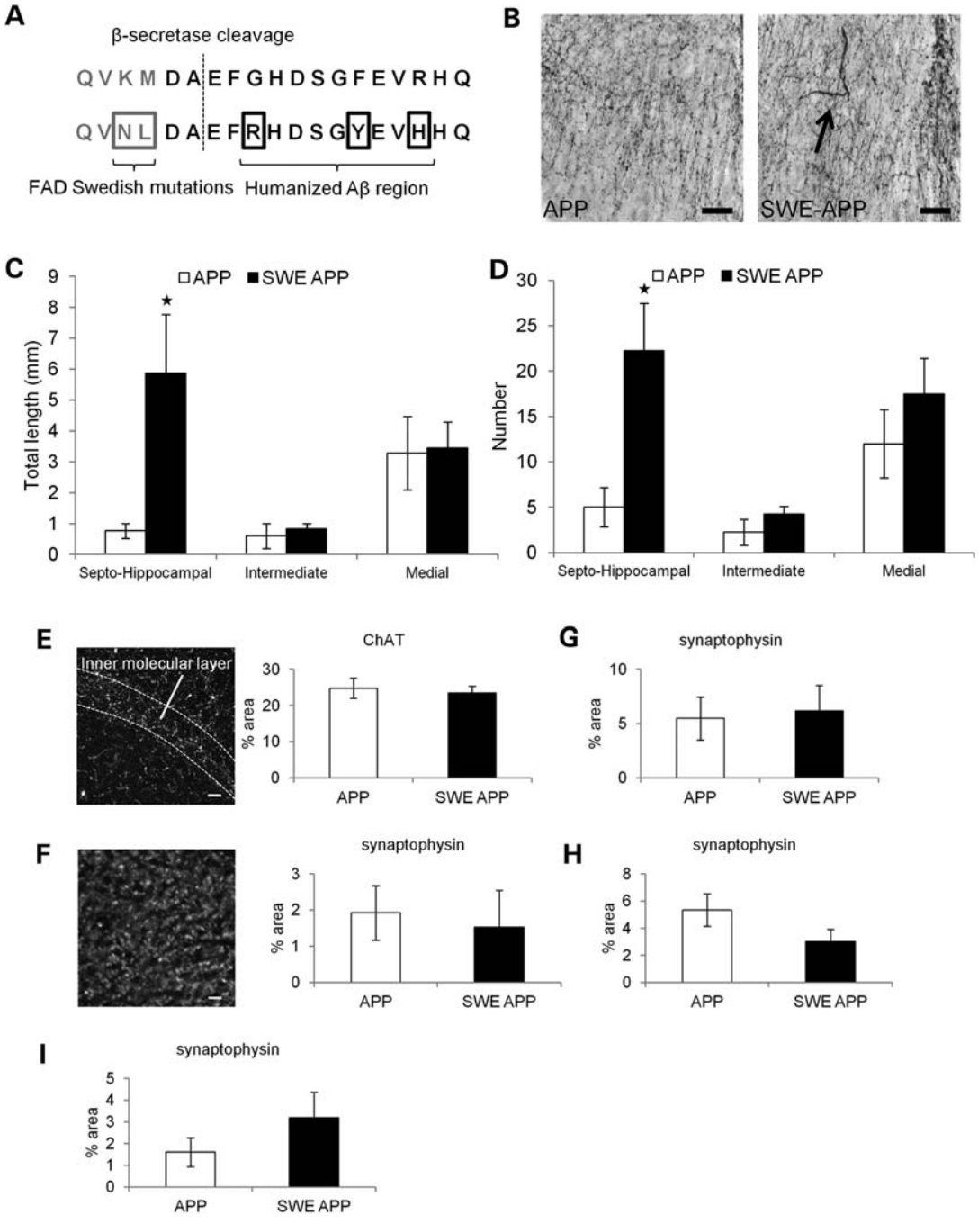

Figure 6. Axonal defects in FAD Swedish APP gene-targeted mice. (**A**) WT (top) and mutant (bottom) amino acid sequences near the β-secretase cleavage site for mouse APP. Mutated amino acids are boxed in the bottom row. (**B**) ChAT immunohistochemistry in the septohippocampal subregion of the septal nucleus in the basal forebrain. Dilated axon (arrow) shown in the FAD Swedish APP brain. Scale bar = 30 μm. (**C**) The average length and (**D**) the average number of dilated axons with diameter over 1.5 μm in septohippocampal, intermediate and medial subregions of the septal nucleus at 12 months [WT, $n = 4$ (white); APP, $n = 4$ (black)]. (**E**) (Left) Example image of ChAT staining in the dentate gyrus of the hippocampus. (Right) The average percent area labeled by ChAT in inner molecular layer of the dentate gyrus in 18 m mice [WT, $n = 4$ (white); APP, $n = 4$ (black)]. (**F**) (Left) Example image of synaptophysin staining in the dentate gyrus. (Right) The average percent area labeled by synaptophysin in the inner molecular layer of dentate gyrus in 6 m mice (WT, $n = 4$; APP, $n = 3$) and (**G**) 18 m mice (WT, $n = 3$; APP, $n = 4$). The average percent area labeled by synaptophysin in the hippocampal region (**H**) CA1 in 18 m mice (WT, $n = 3$; APP, $n = 4$) and (**I**) CA3 in 24 m mice (WT, $n = 3$; APP, $n = 3$) (Mann–Whitney rank-sum test, $^*\alpha < 0.05$).

Swedish APP gene-targeted mice occurs in the absence of other AD-associated pathology, such as synaptic loss and amyloid plaque deposition, and likely represents one of the earliest events in the pathological cascade of disease progression.

DISCUSSION

We investigated the effects of β-secretase cleavage on APP axonal transport and axonal morphology. FAD Swedish

mutations of APP that enhance β-secretase cleavage were sufficient to impair APP anterograde axonal transport *in vitro* and lead to axonal defects *in vivo*. An opposing MV mutation that inhibits the β-cleavage of APP had the opposite effect and stimulated APP anterograde transport, as did the pharmacological inhibition of β-secretase activity. Increasing βCTF and reducing Aβ levels with a γ-secretase inhibitor further reduced Swedish APP anterograde transport, and direct examination of βCTFs revealed dramatic impairment of axonal transport. Taken together, these observations suggest a βCTF-dependent mechanism to impair APP anterograde transport. Furthermore, the brains of mice with FAD Swedish mutations targeted to the mouse APP gene also developed axonal defects in the absence of synaptic degradation or amyloid plaque formation, arguing for axonal changes as an early event in disease progression.

The enhanced β-secretase cleavage of APP was previously suggested to lead to axonal transport defects (10,37), but it was not possible to distinguish effects of APP overexpression from effects of the Swedish mutations that the stimulate β-cleavage of APP. Although a previous study reported that FAD Swedish mutations do not impair APP axonal transport by the criterion of APP accumulation at the proximal side of a nerve ligation, the data demonstrated an increased ratio of retrograde to the anterograde axonal transport of FAD Swedish mutant APP compared with non-mutant APP (45), which is consistent with our findings. In fact, this previous biochemical experiment also provided only an indirect comparison between mice with overexpressed FAD Swedish human APP and mice overexpressing human PS1, an APP processing component, but with endogenous mouse APP (45). Our study made a direct comparison between non-mutant and FAD Swedish mutant human APP, both expressed at similar levels and with endogenously expressed, non-mutant proteolytic processing components. Live imaging of real-time axonal transport demonstrated that FAD Swedish mutations increasing β-secretase cleavage can modestly impair the anterograde axonal transport of APP itself. Identifying the more moderate consequences of the enhanced β-secretase cleavage of APP can, in principle, help elucidate potentially important phenotypes relevant to neurodegeneration. Disease takes decades to develop, especially in late-onset AD, in which there is enhanced APP processing in the absence of APP mutations.

Earlier studies have suggested the divergent axonal transport of CTFs and full-length APP based on their distribution into distinct axonal transport vesicles (8,9). We now provide for the first time a detailed comparative analysis of CTF live axonal transport behavior that supports the qualitative data previously available. We directly examined βCTF axonal transport to demonstrate a dramatic reduction in anterograde transport compared with full-length APP. Increased βCTF levels caused by FAD Swedish mutations of APP likely underlie the comparatively moderate transport phenotype resulting from the mutations. This interpretation is supported by the finding that increasing βCTF levels by using a γ-secretase inhibitor on FAD Swedish APP also severely reduced anterograde transport. Conversely, preventing the β-cleavage of FAD Swedish APP with a β-secretase inhibitor produced a large increase in APP anterograde axonal transport. A sizeable increase in anterograde transport was also seen with MV mutant APP, in which β-cleavage is precluded. Thus, not only does β-secretase cleavage appear to mediate APP axonal transport, but the magnitude of β-secretase cleavage directs the size of the effect on APP axonal transport. Our data indicate that full-length APP has an increased propensity toward anterograde axonal transport toward the synapse than βCTFs.

Several studies report that Aβ can induce defects in the axonal transport of mitochondria and dense core vesicles, and these Aβ-dependent effects appear to target general axonal transport machinery. The total number of transporting vesicles decreased, and both anterograde and retrograde transport and velocities were similarly decreased (26–32,35,36). Our data, on the other hand, provide evidence that mutations affecting APP processing at the β-secretase cleavage site altered the axonal transport of APP itself. There was no decrease in the total number of transporting vesicles, and anterograde and retrograde transport were altered in an opposing manner. Furthermore, the reduced anterograde axonal transport of FAD Swedish APP could be reversed with β-secretase inhibition and exacerbated with γ-secretase inhibition. Because the γ-secretase inhibition of FAD Swedish APP increases βCTF and reduces Aβ production, our data suggest that there is also a βCTF-dependent and Aβ-independent mechanism for APP axonal transport inhibition. In fact, the direct examination of βCTF axonal transport demonstrated that βCTFs have a higher propensity toward retrograde axonal transport compared with full-length APP. Our findings are consistent with previous research that found Aβ-independent defects in axonal transport (2,24,37), in addition to βCTF-dependent and Aβ-independent endosomal changes (21).

The β-secretase cleavage of APP is thought to occur in early endosomes (3,46,47), and endosomes become enlarged upon increased βCTF levels (21) and as an early phenotype in AD (22). In axon terminals of mice carrying an extra copy of the APP gene, early endosomes containing APP, CTFs and the neurotrophic factor nerve growth factor (NGF) were enlarged. Retrograde axonal transport of NGF decreased proportionally with increasing CTF, but not APP, levels, and NGF retrograde axonal transport also decreased in Tg-swAPP^{Prp} mice (24). Because *Drosophila* and mouse models that overexpress either mutant or WT APP exhibit axonal transport defects (2,10,24), it suggests that perturbations to APP processing and amount are both capable of affecting axonal transport. This may be crucial in understanding mechanisms that can contribute to sporadic or late-onset AD, in which there are no mutations to APP. Sporadic AD brains exhibit phenotypes suggestive of axonal transport defects (10) and undergo enhanced APP processing, even though there are no known genetic mutations.

Impaired axonal transport and endosomal defects have been shown to develop concurrently (24) and exhibit βCTF-dependence (21), suggesting a potential mechanistic link. Endosomes in both cell bodies and axon termini have been proposed to play a role in sorting and assembly of APP transport vesicles (48–51). Decreased activity of endosomal component rab3A has previously been reported to reduce the association of APP transport vesicles with motor protein kinesin-I and decrease APP transport into neurites (48). In

light of these findings, it is possible that dysfunctional endosomal activity, caused by the enhanced β-secretase processing of APP and increased βCTF levels, can lead to altered APP transport in both the anterograde and retrograde directions.

A variety of neurodegenerative diseases are associated with defects in axonal transport (52–56), but the initial pathways leading to signs of defective axonal transport in AD remain unknown (10). APP is important for maintaining axonal structure in development and degeneration (57–59). FAD Swedish mutations enhancing the β-secretase cleavage of APP not only impair APP anterograde axonal transport *in vitro*, but they also lead to axonal defects *in vivo* in both gene-targeted mice examined in this study and Tg-swAPP^{Prp} mice previously studied (10). Swedish APP gene-targeted mice develop dilated axons in the cholinergic basal forebrain in the absence of amyloid plaques. While axonal dystrophy is a phenotype commonly associated with amyloid plaques (38–42,60), it has been shown that axonal transport and dystrophy defects can develop well before amyloid plaques deposit in sporadic AD brains (10). Dilated neurites and axon terminals with accumulated proteins have previously been reported independent of, or prior to, plaque deposition (41,60,61). In addition, *Drosophila* and mice overexpressing FAD Swedish APP also develop axonal dystrophy phenotypes typical of axonal transport defects in the absence of plaques (2,10). Because FAD Swedish APP gene-targeted mice have increased levels of both βCTFs and Aβ (43), however, further study is required to address which is responsible for the axonal defects observed and if axonal transport defects are involved.

APP processing has been shown to be important for synaptic signaling and plasticity, both of which have been shown to be impaired in AD and animal models of amyloid pathology (32,48,51,62–74). We demonstrated that FAD Swedish mutations to APP impair APP axonal transport and lead to axonal defects. Abnormal delivery, function and signaling of APP, CTFs and other co-transported factors in axonal vesicles could also potentially compromise synaptic function as a downstream effect. Previous studies report that primary neuronal cultures from FAD mutant mice had inhibited the transport of mitochondria and reduced synaptic proteins (36,68). The gene-targeted FAD Swedish mice in our study, however, develop axonal defects without any detectable corresponding synaptic loss. The axonal defects we report likely represent an early event, while synaptic damage and neuronal dysfunction occur later in the pathological process. Gene-targeted mice have normal levels of APP expression without plaque formation and might capture early disease progression, while transgenic mice that overexpress FAD mutant proteins and eventually form plaques likely represent an accelerated pathological process.

The possible significance of altered APP axonal transport caused by FAD mutations is highlighted by the findings that defective axonal transport can contribute to the development of both AD-related amyloid and tau pathology (10,75). When axonal transport was further disrupted in Tg-swAPP^{Prp} mice by reducing kinesin motor protein subunit kinesin light chain 1 (KLC1), Aβ levels and amyloid plaque deposition increased (10). Axonal injury also causes APP and fragments, including Aβ, to accumulate at sites of damage (76–80). Thus, assaults to axonal health, such as defective axonal transport, can contribute to the amyloidogenic processing of APP or amyloid deposition. Furthermore, axonal transport defects in mice lacking KLC1 lead to abnormal tau hyperphosphorylation and accumulation, along with axonal swellings and activation of stress kinases (75). Tau hyperphosphorylation underlies the neurofibrillary tangle formation associated with AD. Reducing KLC1 in animal models of tauopathy also exacerbates tau hyperphosphorylation, aggregation and neurodegeneration (81). Thus, transport inhibition can contribute to tau pathology. Together, these findings suggest that impaired axonal transport could potentially contribute to disease progression by increasing amyloidogenesis and abnormal tau phosphorylation as a downstream effect. Amyloidogenesis and abnormal tau phosphorylation could, in turn, eventually further disrupt general axonal transport mechanisms (9,27,82,83), presenting a possible cascade of events toward cellular demise and pathology characterizing AD. These findings continue to underscore the importance of possible Aβ-independent, as well as Aβ-dependent, disease mechanisms driven by APP and its cleavage products that result from the enhanced β-secretase cleavage of APP in sporadic and FAD.

MATERIALS AND METHODS

Constructs

Bacterial plasmid pcDNA3 uses a cytomegalovirus promoter to encode for APP695 with YFP fused to the C terminus (APP-YFP) (84). With the use of QuikChange II XL site-directed mutagenesis kit (Stratagene), mutations were targeted to the amino acids immediately adjacent to the β-secretase cleavage site of APP to create two new constructs. The first mutant construct contained the FAD Swedish mutations (K595N and M596L), while the second mutant construct contained the MV mutation (M596V). To create αCTF-EGFP (C83-EGFP), a βCTF-EGFP (C99-EGFP) construct, graciously obtained in a pcDNA3.1 vector from C. Haass (85), was used as the starting construct for a two-step cloning procedure. The C83 fragment with the signal peptide and C-terminal EGFP were then cloned into a pcDNA3 vector. APP-EGFP was a generous gift from O.M. Andersen (unpublished data). Several preparations of each plasmid were used for experiments.

Cultures

Primary hippocampal cultures were prepared by dissecting brains from WT, newborn C57BL/J6 mice on post-natal day 1. Dissection buffer consisted of Hank's Balanced Salt Solution with glucose, hydroxyethyl piperazineethanesulfonic acid and antibiotics. Isolated hippocampi were incubated in a 0.22 μm filtered mixture of 45 U papain (Worthington) in phosphate-buffered saline (PBS), DL-cystein HCl (Sigma), bovine serum albumin and D-glucose (Sigma) enriched with 0.05% of DNase (Boehringer Mannheim) for 20 min at 37°C. Hippocampi were triturated by pipetting carefully in Dulbecco's Modified Eagle Medium with 10% fetal bovine serum (FBS). Cells were grown in 500 μM L-glutamine and neurobasal media supplemented with B27 (Invitrogen) over

poly-L-lysine-coated coverslips and stored in a 37°C incubator with 5% CO_2. At least three separate cultures prepared on different days were used for each experiment. SH-SY5Y cultures were grown in F-12 nutrient and Hamm media supplemented with 10% FBS.

Transfection and drug treatment

After 10 days in culture, hippocampal neurons were transfected with APP-YFP for 2 h with 800 ng of WT or mutant DNA per well of a 24-well plate. Low transfection efficiency was obtained using Lipofectamine 2000 (Invitrogen). Experiments were designed to collect data 12–16 h after transfection from control and experimental groups in parallel. From a single 24-well plate of cultured hippocampal neurons, half the wells were transfected with WT APP-YFP, while the other half was transfected with mutant APP-YFP. Transfected hippocampal cultures in some experiments were treated with either β-secretase inhibitor II (Calbiochem) or γ-secretase inhibitor compound E (Calbiochem). For drug treatment experiments, the entire plate was transfected with either Swedish or MV APP-YFP. An hour before imaging the next day, half the wells were treated with drug dissolved in dimethyl sulfoxide (DMSO), and half the wells were treated with an equal volume of DMSO only. For APP-, βCTF- and αCTF-EGFP transfections, 500 ng of DNA was used per well, and data were collected 4–10 h after transfection. At least three separate culture preparations and transfections were performed for each experimental group, using multiple preparations of plasmid DNA. SH-SY5Y cells were used for western blot experiments because of their high transfection efficiency. Transfections the day after splitting followed a protocol similar to hippocampal transfection.

Axonal APP-YFP movie collection

Transfected axons were located in primary hippocampal cultures using an inverted epifluorescent microscope (TE-2000U, Nikon) and a 100× oil immersion objective (Nikon, 1.4 NA, 0.126 μm/pixel) connected to a CCD camera (Roper Scientific). During imaging, cultures were kept at 37°C using a heated stage and 5% CO_2 chamber. Twelve to 16 h after transfection, movies of axons expressing fluorescent protein were collected using Metamorph 7.0 software (Universal Imaging Corporation) run on a PC computer. Directionality was determined by tracking axons far away from cell bodies or axon termini, and individual transfected axons could be distinguished due to the small number of transfected neurons in the primary culture. Data were not collected if movement directionality could not be determined, or if cells appeared unhealthy. Particles moving from cell bodies to axon termini were considered anterograde, and those moving from termini to cell bodies were considered retrograde. Continuous, 15-second movies of 150 frames with 100 millisecond exposure for each frame were collected for APP-YFP or APP-EGFP axonal movement. Phase and fluorescent images of cell bodies were also collected to ensure that there were no signs of gross toxicity to the cells or substantial differences in the amount of transfected fluorescent protein present. All movies were collected within an hour of the culture being placed in the heat- and CO_2-controlled microscope incubator chamber.

APP-YFP movement analysis

Using Metamorph software, a kymograph was generated for each movie to plot time on the *y*-axis and distance on the *x*-axis for the movement of each fluorescent particle. Manual analyses were conducted on particle movement trajectories plotted on these kymographs. Percentages of anterograde, retrograde and stationary particles were extracted by following particle movement from initial starting point to ultimate ending point along the kymographs. Segmental velocity and run length are the speed and distance a particle travels in a given direction, during a segment of movement that is not interrupted by a pause in movement or a reversal in movement direction. These were calculated using kymographs by tracing particle movement across an uninterrupted segment of movement, then calculating distance traveled and time taken to travel that distance. Each data set analyzed consists of movies collected from at least three separate culture preparations and transfections performed on different days, using multiple plasmid preparations. Only data from multiple repetitions of these experiments performed in parallel on several different days were pooled for analyses.

Western blot analysis

Protein analysis of transfected cultures was performed by western blots. For each experiment, one 10 cm plate of SH-SY5Y cells was transfected with each construct. The next day, cells were rinsed of culture media and scraped from the plate using PBS with a protease inhibitor cocktail (Roche). Cells were collected on ice, and then pelleted by centrifuging at 4°C for 10 min at 1000*g*. After removing PBS, the cell pellets were resuspended and homogenized using NP-40 lysis buffer. After protein concentration was determined using the Bradford assay, an equal volume of 2× lithium dodecyl sulfate sample buffer (Invitrogen) was added with β-mercaptoethanol to a final concentration of 4%. Equal amounts of protein samples were loaded onto 4–12% Bis–Tris gels, using SeePlus 2 as a molecular weight marker (Invitrogen), and gels ran at 90 V until dye reached the end of the gel. Transfer onto nitrocellulose membranes was done at 0.3 A for 90 min using 25 mM Tris-base, 190 mM glycine and 20% methanol. Ponceau S stain (Sigma) indicated the quality of the transfer and was used as a guide when cutting membranes into separate sections for incubation with different antibodies. Membrane blocking was performed for 1 h at room temperature with 5% milk in Tris-buffered saline with 0.25% Tween (TBST), while primary antibody diluted in blocking solution was incubated overnight at 4°C. Human-specific APP antibody 6E10 (Covance) was used at 1:1000. This antibody recognizes the first 16 amino acids of the Aβ region and will consequently detect full-length APP and βCTFs, but not αCTFs. C-terminal APP antibody (Zymed) was used at 1:500 to detect αCTF. Tubulin was used at 1:10 000 as a loading control. Antibodies were used sequentially to detect levels of βCTF-YFP and tubulin in the same membrane.

Horseradish peroxidase-conjugated goat anti-mouse IgG secondary antibody was diluted in TBST at 1:10 000, and incubation was done for 2 h at room temperature. Membranes were developed with ECL Western blotting substrate (Pierce). Dissected mouse brains were collected and immediately frozen in liquid nitrogen. Sample preparation and western blot technique were performed in a similar fashion.

Mice and genetic crosses

Gene-targeted mice obtained for these studies possess FAD Swedish mutations and a humanized Aβ region targeted to the mouse APP gene and were originally on the 129/CD-1 genetic background (Cephalon, West Chester, PA, USA) (42). We backcrossed these mice onto the C57BL/J6 genetic background for five generations and bred to each other the resulting C57BL/J6 mice heterozygous for the gene-targeted APP mutations. Mice homozygous for the APP gene-targeted mutations and their age-matched, WT littermates were included for study.

Immunohistochemistry

At various ages, mice were transcardially perfused first with 0.1 M phosphate buffer (PB), pH 7.2, followed by 4% paraformaldehyde in PB (4% PFA). Dissected brains were post-fixed overnight with 4% PFA at 4°C. Coronal sections 50 μm thick were cut using a vibrating blade microtome (Leica 1000S), collected in PB and stored in 30% glycerol cryoprotectant until immunohistochemistry was performed the next day. For light microscopy, every 6th section was collected in PB into a serially sampled set representative of the cholinergic basal forebrain and rinsed in PB three times for 5 min each rinse. Brain slices there then quenched for 1 h at room temperature with 0.6% hydrogen peroxide and rinsed again in PB. Tissue was blocked and permeabilized for 1 h at room temperature with 10% serum and 0.2% Triton X-100 in PB, then incubated in primary antibody ChAT (Invitrogen) diluted 1:100 in the same solution for 72 h at 4°C. After washing brain sections with PB six times for 10 min each rinse, tissue was blocked again. Primary antibody signal was enhanced using a biotinylated secondary antibody (Jackson ImmunoResearch) at 1:200 for 1 h at room temperature, followed by rinsing with PB. Tissue was then incubated with biotin–avidin complexes from the ABC vectastain kit for 1 h at room temperature, rinsed and developed with Nova Red (Vector Laboratories). After rinsing with water and mounting onto microscope slides, brain slices were dehydrated in an ethanol series, cleared with xylene and mounted with Permount (Fisher). Slides were then coded for blind data collection and analysis using a stereological approach. Fluorescence microscopy was conducted in a fashion similar to light microscopy. Three serial sections through the hippocampus for each mouse were collected in PB, rinsed, blocked and permeabilized, then incubated in either primary antibody synaptophysin (Millipore) or ChAT (Invitrogen) at 1:100 overnight at 4°C. After washing brain sections with PB three times for 5 min each rinse, they were incubated with a fluorophore-conjugated secondary (AlexaFluor) at 1:200 for 1 h at room temperature. Tissue was mounted with fluorescence-preserving Vectashield media (Vector Laboratories).

Stereology

Brain stereology was performed with an Axioplan Zeiss light microscope associated with a Bioquant Nova Stereology software image analysis system (Bioquant R&M Biometrics, Inc.). In brief, dystrophic cholinergic axon length and number were determined using random, systematically-sampled serial sections of 50 μm brain slices. The first slice was selected as the most anterior slice containing the septal nucleus, with every other slice spaced apart by 250 μm. Random serial sections were analyzed using the Bioquant system to calculate lengths and numbers of dystrophic axons by tracing non-varicose, dilated axons with widths over 1.5 μm in the entire area of each septal nucleus subregion contained in each brain slice. A minimum of three mice per experimental group were analyzed at each age point.

Immunofluorescent analyses

Fluorescent images were collected with an inverted Nikon Bio-Rad Laboratories FV-1000 confocal imaging system and 100× oil immersion objective. Before data collection, confocal acquisition settings to be used for all images were determined to ensure for an intensity range below saturation. Images were collected at six different sites within the synaptic region of interest for each brain slice. Single images were collected for synaptophysin at each location. For ChAT imaging, z stacks were collected, consisting of 10 images separated by 1 μm, and made into maximum projections. Analysis consisted of using ImageJ software to apply a standard threshold selection to all synaptophysin or all ChAT images and calculate the percent area labeled. Mean values were obtained for each animal, and animals within the same genotype were pooled for statistical analyses and graphical plotting.

Statistics

For analyses of APP-YFP movement parameters, Student's *t*-tests were used to determine significant differences between mutant and WT, or drug-treated and vehicle-treated, groups. Percentages of movement in each direction, mean segmental velocities and mean segmental run lengths were calculated for each movie collected. These movie values were used for statistical comparisons between experimental groups. Single stars indicate statistical significance with a *P*-value of <0.05, and double stars indicate a *P*-value of <0.01. Graphs plot the percent of the control value for each construct or drug-treatment group, and error bars represent the standard error of the mean (SEM). For analyses of gene-targeted mice, each graph plots genotype means obtained from several animals, and error bars represent the SEM. Asterisks indicate statistical significance. For brain stereology and immunofluorescent image analyses, a Mann–Whitney (two sample rank sum) nonparametric statistical test was used at an α significance of 0.05.

ACKNOWLEDGEMENTS

We would like to thank C. Haass for the C99-EGFP plasmid construct and O.M. Andersen for the APP-EGFP plasmid construct.

Conflict of Interest statement. None declared.

FUNDING

This work was supported by National Institutes of Health (AG032180 to L.S.B.G., AG027688 to E.M.R. and 2PN2EY16525, NS24054, NS055371 to A.M.W., provided to W.C. Mobley).

REFERENCES

1. Papp, H., Pakaski, M. and Kasa, P. (2002) Presenilin-1 and the amyloid precursor protein are transported bidirectionally in the sciatic nerve of adult rat. *Neurochem. Int.*, **41**, 429–435.
2. Gunawardena, S. and Goldstein, L.S. (2001) Disruption of axonal transport and neuronal viability by amyloid precursor protein mutations in *Drosophila*. *Neuron*, **32**, 389–401.
3. Yamazaki, T., Selkoe, D.J. and Koo, E.H. (1995) Trafficking of cell surface beta-amyloid precursor protein: retrograde and transcytotic transport in cultured neurons. *J. Cell Biol.*, **129**, 431–442.
4. Sisodia, S.S., Koo, E.H., Hoffman, P.N., Perry, G. and Price, D.L. (1993) Identification and transport of full-length amyloid precursor proteins in rat peripheral nervous system. *J. Neurosci.*, **13**, 3136–3142.
5. Koo, E.H., Sisodia, S.S., Archer, D.R., Martin, L.J., Weidemann, A., Beyreuther, K., Fischer, P., Masters, C.L. and Price, D.L. (1990) Precursor of amyloid protein in Alzheimer disease undergoes fast anterograde axonal transport. *Proc. Natl Acad. Sci. USA*, **87**, 1561–1565.
6. Buxbaum, J.D., Thinakaran, G., Koliatsos, V., O'Callahan, J., Slunt, H.H., Price, D.L. and Sisodia, S.S. (1998) Alzheimer amyloid protein precursor in the rat hippocampus: transport and processing through the perforant path. *J. Neurosci.*, **18**, 9629–9637.
7. Lazarov, O., Lee, M., Peterson, D.A. and Sisodia, S.S. (2002) Evidence that synaptically released beta-amyloid accumulates as extracellular deposits in the hippocampus of transgenic mice. *J. Neurosci.*, **22**, 9785–9793.
8. Muresan, V., Varvel, N.H., Lamb, B.T. and Muresan, Z. (2009) The cleavage products of amyloid-beta precursor protein are sorted to distinct carrier vesicles that are independently transported within neurites. *J. Neurosci.*, **29**, 3565–3578.
9. Goldsbury, C., Mocanu, M.M., Thies, E., Kaether, C., Haass, C., Keller, P., Biernat, J., Mandelkow, E. and Mandelkow, E.M. (2006) Inhibition of APP trafficking by tau protein does not increase the generation of amyloid-beta peptides. *Traffic*, **7**, 873–888.
10. Stokin, G.B., Lillo, C., Falzone, T.L., Brusch, R.G., Rockenstein, E., Mount, S.L., Raman, R., Davies, P., Masliah, E., Williams, D.S. *et al.* (2005) Axonopathy and transport deficits early in the pathogenesis of Alzheimer's disease. *Science*, **307**, 1282–1288.
11. Bowman, A.B., Kamal, A., Ritchings, B.W., Philp, A.V., McGrail, M., Gindhart, J.G. and Goldstein, L.S. (2000) Kinesin-dependent axonal transport is mediated by the Sunday driver (SYD) protein. *Cell*, **103**, 583–594.
12. Bowman, A.B., Patel-King, R.S., Benashski, S.E., McCaffery, J.M., Goldstein, L.S. and King, S.M. (1999) *Drosophila roadblock* and *Chlamydomonas* LC7: a conserved family of dynein-associated proteins involved in axonal transport, flagellar motility, and mitosis. *J. Cell Biol.*, **146**, 165–180.
13. Martin, M., Iyadurai, S.J., Gassman, A., Gindhart, J.G. Jr, Hays, T.S. and Saxton, W.M. (1999) Cytoplasmic dynein, the dynactin complex, and kinesin are interdependent and essential for fast axonal transport. *Mol. Biol. Cell*, **10**, 3717–3728.
14. Torroja, L., Chu, H., Kotovsky, I. and White, K. (1999) Neuronal overexpression of APPL, the *Drosophila* homologue of the amyloid precursor protein (APP), disrupts axonal transport. *Curr. Biol.*, **9**, 489–492.
15. Gindhart, J.G. Jr, Desai, C.J., Beushausen, S., Zinn, K. and Goldstein, L.S. (1998) Kinesin light chains are essential for axonal transport in *Drosophila*. *J. Cell Biol.*, **141**, 443–454.
16. Hurd, D.D. and Saxton, W.M. (1996) Kinesin mutations cause motor neuron disease phenotypes by disrupting fast axonal transport in *Drosophila*. *Genetics*, **144**, 1075–1085.
17. Haass, C., Lemere, C.A., Capell, A., Citron, M., Seubert, P., Schenk, D., Lannfelt, L. and Selkoe, D.J. (1995) The Swedish mutation causes early-onset Alzheimer's disease by beta-secretase cleavage within the secretory pathway. *Nat. Med.*, **1**, 1291–1296.
18. Evin, G., Zhu, A., Holsinger, R.M., Masters, C.L. and Li, Q.X. (2003) Proteolytic processing of the Alzheimer's disease amyloid precursor protein in brain and platelets. *J. Neurosci. Res.*, **74**, 386–392.
19. Yang, L.B., Lindholm, K., Yan, R., Citron, M., Xia, W., Yang, X.L., Beach, T., Sue, L., Wong, P., Price, D. *et al.* (2003) Elevated beta-secretase expression and enzymatic activity detected in sporadic Alzheimer disease. *Nat. Med.*, **9**, 3–4.
20. Holsinger, R.M., McLean, C.A., Beyreuther, K., Masters, C.L. and Evin, G. (2002) Increased expression of the amyloid precursor beta-secretase in Alzheimer's disease. *Ann. Neurol.*, **51**, 783–786.
21. Jiang, Y., Mullaney, K.A., Peterhoff, C.M., Che, S., Schmidt, S.D., Boyer-Boiteau, A., Ginsberg, S.D., Cataldo, A.M., Mathews, P.M. and Nixon, R.A. (2010) Alzheimer's-related endosome dysfunction in Down syndrome is Abeta-independent but requires APP and is reversed by BACE-1 inhibition. *Proc. Natl Acad. Sci. USA*, **107**, 1630–1635.
22. Cataldo, A.M., Peterhoff, C.M., Troncoso, J.C., Gomez-Isla, T., Hyman, B.T. and Nixon, R.A. (2000) Endocytic pathway abnormalities precede amyloid beta deposition in sporadic Alzheimer's disease and Down syndrome: differential effects of APOE genotype and presenilin mutations. *Am. J. Pathol.*, **157**, 277–286.
23. Rusu, P., Jansen, A., Soba, P., Kirsch, J., Lower, A., Merdes, G., Kuan, Y.H., Jung, A., Beyreuther, K., Kjaerulff, O. *et al.* (2007) Axonal accumulation of synaptic markers in APP transgenic *Drosophila* depends on the NPTY motif and is paralleled by defects in synaptic plasticity. *Eur. J. Neurosci.*, **25**, 1079–1086.
24. Salehi, A., Delcroix, J.D., Belichenko, P.V., Zhan, K., Wu, C., Valletta, J.S., Takimoto-Kimura, R., Kleschevnikov, A.M., Sambamurti, K., Chung, P.P. *et al.* (2006) Increased App expression in a mouse model of Down's syndrome disrupts NGF transport and causes cholinergic neuron degeneration. *Neuron*, **51**, 29–42.
25. Kamal, A., Stokin, G.B., Yang, Z., Xia, C.H. and Goldstein, L.S. (2000) Axonal transport of amyloid precursor protein is mediated by direct binding to the kinesin light chain subunit of kinesin-I. *Neuron*, **28**, 449–459.
26. Rui, Y., Tiwari, P., Xie, Z. and Zheng, J.Q. (2006) Acute impairment of mitochondrial trafficking by beta-amyloid peptides in hippocampal neurons. *J. Neurosci.*, **26**, 10480–10487.
27. Vossel, K.A., Zhang, K., Brodbeck, J., Daub, A.C., Sharma, P., Finkbeiner, S., Cui, B. and Mucke, L. (2010) Tau reduction prevents Aβ-induced defects in axonal transport. *Science*, **330**, 198.
28. Decker, H., Lo, K.Y., Unger, S.M., Ferreira, S.T. and Silverman, M.A. (2010) Amyloid-beta peptide oligomers disrupt axonal transport through an NMDA receptor-dependent mechanism that is mediated by glycogen synthase kinase 3beta in primary cultured hippocampal neurons. *J. Neurosci.*, **30**, 9166–9171.
29. Pigino, G., Morfini, G., Atagi, Y., Deshpande, A., Yu, C., Jungbauer, L., LaDu, M., Busciglio, J. and Brady, S. (2009) Disruption of fast axonal transport is a pathogenic mechanism for intraneuronal amyloid beta. *Proc. Natl Acad. Sci. USA*, **106**, 5907–5912.
30. Hiruma, H., Katakura, T., Takahashi, S., Ichikawa, T. and Kawakami, T. (2003) Glutamate and amyloid beta-protein rapidly inhibit fast axonal transport in cultured rat hippocampal neurons by different mechanisms. *J. Neurosci.*, **23**, 8967–8977.
31. Kasa, P., Papp, H., Kovacs, I., Forgon, M., Penke, B. and Yamaguchi, H. (2000) Human amyloid-beta1-42 applied in vivo inhibits the fast axonal transport of proteins in the sciatic nerve of rat. *Neurosci. Lett.*, **278**, 117–119.
32. Calkins, M.J. and Reddy, P.H. (2011) Amyloid beta impairs mitochondrial anterograde transport and degenerates synapses in Alzheimer's disease neurons. *Biochim. Biophys. Acta*, **1812**, 507–513.

33. Mullan, M., Crawford, F., Axelman, K., Houlden, H., Lilius, L., Winblad, B. and Lannfelt, L. (1992) A pathogenic mutation for probable Alzheimer's disease in the APP gene at the N-terminus of beta-amyloid. *Nat. Genet.*, **1**, 345–347.
34. Citron, M., Teplow, D.B. and Selkoe, D.J. (1995) Generation of amyloid beta protein from its precursor is sequence specific. *Neuron*, **14**, 661–670.
35. Cai, D., Leem, J.Y., Greenfield, J.P., Wang, P., Kim, B.S., Wang, R., Lopes, K.O., Kim, S.H., Zheng, H., Greengard, P. *et al.* (2003) Presenilin-1 regulates intracellular trafficking and cell surface delivery of beta-amyloid precursor protein. *J. Biol. Chem.*, **278**, 3446–3454.
36. Pigino, G., Morfini, G., Pelsman, A., Mattson, M.P., Brady, S.T. and Busciglio, J. (2003) Alzheimer's presenilin 1 mutations impair kinesin-based axonal transport. *J. Neurosci.*, **23**, 4499–4508.
37. Stokin, G.B., Almenar-Queralt, A., Gunawardena, S., Rodrigues, E.M., Falzone, T., Kim, J., Lillo, C., Mount, S.L., Roberts, E.A., McGowan, E. *et al.* (2008) Amyloid precursor protein-induced axonopathies are independent of amyloid-beta peptides. *Hum. Mol. Genet.*, **17**, 3474–3486.
38. Schmidt, M.L., DiDario, A.G., Lee, V.M. and Trojanowski, J.Q. (1994) An extensive network of PHF tau-rich dystrophic neurites permeates neocortex and nearly all neuritic and diffuse amyloid plaques in Alzheimer disease. *FEBS Lett.*, **344**, 69–73.
39. Masliah, E., Mallory, M., Deerinck, T., DeTeresa, R., Lamont, S., Miller, A., Terry, R.D., Carragher, B. and Ellisman, M. (1993) Re-evaluation of the structural organization of neuritic plaques in Alzheimer's disease. *J. Neuropathol. Exp. Neurol.*, **52**, 619–632.
40. Lenders, M.B., Peers, M.C., Tramu, G., Delacourte, A., Defossez, A., Petit, H. and Mazzuca, M. (1989) Dystrophic neuropeptidergic neurites in senile plaques of Alzheimer's disease precede formation of paired helical filaments. *Acta Neurol. Belg.*, **89**, 279–285.
41. Braak, H., Braak, E., Grundke-Iqbal, I. and Iqbal, K. (1986) Occurrence of neuropil threads in the senile human brain and in Alzheimer's disease: a third location of paired helical filaments outside of neurofibrillary tangles and neuritic plaques. *Neurosci. Lett.*, **65**, 351–355.
42. Selkoe, D.J. (1986) Altered structural proteins in plaques and tangles: what do they tell us about the biology of Alzheimer's disease? *Neurobiol. Aging*, **7**, 425–432.
43. Reaume, A.G., Howland, D.S., Trusko, S.P., Savage, M.J., Lang, D.M., Greenberg, B.D., Siman, R. and Scott, R.W. (1996) Enhanced amyloidogenic processing of the beta-amyloid precursor protein in gene-targeted mice bearing the Swedish familial Alzheimer's disease mutations and a 'humanized' Abeta sequence. *J. Biol. Chem.*, **271**, 23380–23388.
44. Flood, D.G., Reaume, A.G., Dorfman, K.S., Lin, Y.G., Lang, D.M., Trusko, S.P., Savage, M.J., Annaert, W.G., De Strooper, B., Siman, R. *et al.* (2002) FAD mutant PS-1 gene-targeted mice: increased A beta 42 and A beta deposition without APP overproduction. *Neurobiol. Aging*, **23**, 335–348.
45. Lazarov, O., Morfini, G.A., Pigino, G., Gadadhar, A., Chen, X., Robinson, J., Ho, H., Brady, S.T. and Sisodia, S.S. (2007) Impairments in fast axonal transport and motor neuron deficits in transgenic mice expressing familial Alzheimer's disease-linked mutant presenilin 1. *J. Neurosci.*, **27**, 7011–7020.
46. Yamazaki, T., Koo, E.H. and Selkoe, D.J. (1996) Trafficking of cell-surface amyloid beta-protein precursor. II. Endocytosis, recycling and lysosomal targeting detected by immunolocalization. *J. Cell Sci.*, **109** (Pt 5), 999–1008.
47. Koo, E.H. and Squazzo, S.L. (1994) Evidence that production and release of amyloid beta-protein involves the endocytic pathway. *J. Biol. Chem.*, **269**, 17386–17389.
48. Szodorai, A., Kuan, Y.H., Hunzelmann, S., Engel, U., Sakane, A., Sasaki, T., Takai, Y., Kirsch, J., Muller, U., Beyreuther, K. *et al.* (2009) APP anterograde transport requires Rab3A GTPase activity for assembly of the transport vesicle. *J. Neurosci.*, **29**, 14534–14544.
49. Deinhardt, K., Salinas, S., Verastegui, C., Watson, R., Worth, D., Hanrahan, S., Bucci, C. and Schiavo, G. (2006) Rab5 and Rab7 control endocytic sorting along the axonal retrograde transport pathway. *Neuron*, **52**, 293–305.
50. Delcroix, J.D., Valletta, J., Wu, C., Howe, C.L., Lai, C.F., Cooper, J.D., Belichenko, P.V., Salehi, A. and Mobley, W.C. (2004) Trafficking the NGF signal: implications for normal and degenerating neurons. *Prog. Brain Res.*, **146**, 3–23.
51. Marquez-Sterling, N.R., Lo, A.C., Sisodia, S.S. and Koo, E.H. (1997) Trafficking of cell-surface beta-amyloid precursor protein: evidence that a sorting intermediate participates in synaptic vesicle recycling. *J. Neurosci.*, **17**, 140–151.
52. Roy, S., Zhang, B., Lee, V.M. and Trojanowski, J.Q. (2005) Axonal transport defects: a common theme in neurodegenerative diseases. *Acta Neuropathol.*, **109**, 5–13.
53. LaMonte, B.H., Wallace, K.E., Holloway, B.A., Shelly, S.S., Ascano, J., Tokito, M., Van Winkle, T., Howland, D.S. and Holzbaur, E.L. (2002) Disruption of dynein/dynactin inhibits axonal transport in motor neurons causing late-onset progressive degeneration. *Neuron*, **34**, 715–727.
54. Zhao, C., Takita, J., Tanaka, Y., Setou, M., Nakagawa, T., Takeda, S., Yang, H.W., Terada, S., Nakata, T., Takei, Y. *et al.* (2001) Charcot-Marie-Tooth disease type 2A caused by mutation in a microtubule motor KIF1Bbeta. *Cell*, **105**, 587–597.
55. Reid, E., Kloos, M., Ashley-Koch, A., Hughes, L., Bevan, S., Svenson, I.K., Graham, F.L., Gaskell, P.C., Dearlove, A., Pericak-Vance, M.A. *et al.* (2002) A kinesin heavy chain (KIF5A) mutation in hereditary spastic paraplegia (SPG10). *Am. J. Hum. Genet.*, **71**, 1189–1194.
56. Puls, I., Jonnakuty, C., LaMonte, B.H., Holzbaur, E.L., Tokito, M., Mann, E., Floeter, M.K., Bidus, K., Drayna, D., Oh, S.J. *et al.* (2003) Mutant dynactin in motor neuron disease. *Nat. Genet.*, **33**, 455–456.
57. Nikolaev, A., McLaughlin, T., O'Leary, D.D. and Tessier-Lavigne, M. (2009) APP binds DR6 to trigger axon pruning and neuron death via distinct caspases. *Nature*, **457**, 981–989.
58. Qiu, W.Q., Ferreira, A., Miller, C., Koo, E.H. and Selkoe, D.J. (1995) Cell-surface beta-amyloid precursor protein stimulates neurite outgrowth of hippocampal neurons in an isoform-dependent manner. *J. Neurosci.*, **15**, 2157–2167.
59. Muller, U., Cristina, N., Li, Z.W., Wolfer, D.P., Lipp, H.P., Rulicke, T., Brandner, S., Aguzzi, A. and Weissmann, C. (1994) Behavioral and anatomical deficits in mice homozygous for a modified beta-amyloid precursor protein gene. *Cell*, **79**, 755–765.
60. Gouras, G.K., Almeida, C.G. and Takahashi, R.H. (2005) Intraneuronal Abeta accumulation and origin of plaques in Alzheimer's disease. *Neurobiol. Aging*, **26**, 1235–1244.
61. Takahashi, R.H., Milner, T.A., Li, F., Nam, E.E., Edgar, M.A., Yamaguchi, H., Beal, M.F., Xu, H., Greengard, P. and Gouras, G.K. (2002) Intraneuronal Alzheimer abeta42 accumulates in multivesicular bodies and is associated with synaptic pathology. *Am. J. Pathol.*, **161**, 1869–1879.
62. Moya, K.L., Benowitz, L.I., Schneider, G.E. and Allinquant, B. (1994) The amyloid precursor protein is developmentally regulated and correlated with synaptogenesis. *Dev. Biol.*, **161**, 597–603.
63. Chapman, P.F., White, G.L., Jones, M.W., Cooper-Blacketer, D., Marshall, V.J., Irizarry, M., Younkin, L., Good, M.A., Bliss, T.V., Hyman, B.T. *et al.* (1999) Impaired synaptic plasticity and learning in aged amyloid precursor protein transgenic mice. *Nat. Neurosci.*, **2**, 271–276.
64. Cirrito, J.R., Yamada, K.A., Finn, M.B., Sloviter, R.S., Bales, K.R., May, P.C., Schoepp, D.D., Paul, S.M., Mennerick, S. and Holtzman, D.M. (2005) Synaptic activity regulates interstitial fluid amyloid-beta levels in vivo. *Neuron*, **48**, 913–922.
65. Wang, P., Yang, G., Mosier, D.R., Chang, P., Zaidi, T., Gong, Y.D., Zhao, N.M., Dominguez, B., Lee, K.F., Gan, W.B. *et al.* (2005) Defective neuromuscular synapses in mice lacking amyloid precursor protein (APP) and APP-Like protein 2. *J. Neurosci.*, **25**, 1219–1225.
66. Calabrese, B., Shaked, G.M., Tabarean, I.V., Braga, J., Koo, E.H. and Halpain, S. (2007) Rapid, concurrent alterations in pre- and postsynaptic structure induced by naturally-secreted amyloid-beta protein. *Mol. Cell. Neurosci.*, **35**, 183–193.
67. Tampellini, D., Rahman, N., Gallo, E.F., Huang, Z., Dumont, M., Capetillo-Zarate, E., Ma, T., Zheng, R., Lu, B., Nanus, D.M. *et al.* (2009) Synaptic activity reduces intraneuronal Abeta, promotes APP transport to synapses, and protects against Abeta-related synaptic alterations. *J. Neurosci.*, **29**, 9704–9713.
68. Calkins, M.J., Manczak, M., Mao, P., Shirendeb, U. and Reddy, P.H. (2011) Impaired mitochondrial biogenesis, defective axonal transport of mitochondria, abnormal mitochondrial dynamics and synaptic degeneration in a mouse model of Alzheimer's disease. *Hum. Mol. Genet.*, **20**, 4515–4529.
69. Abramov, E., Dolev, I., Fogel, H., Ciccotosto, G.D., Ruff, E. and Slutsky, I. (2009) Amyloid-beta as a positive endogenous regulator of release probability at hippocampal synapses. *Nat. Neurosci.*, **12**, 1567–1576.

70. Wei, W., Nguyen, L.N., Kessels, H.W., Hagiwara, H., Sisodia, S. and Malinow, R. (2010) Amyloid beta from axons and dendrites reduces local spine number and plasticity. *Nat. Neurosci.*, **13**, 190–196.
71. Masliah, E., Hansen, L., Albright, T., Mallory, M. and Terry, R.D. (1991) Immunoelectron microscopic study of synaptic pathology in Alzheimer's disease. *Acta Neuropathol.*, **81**, 428–433.
72. Masliah, E., Terry, R.D., Alford, M., DeTeresa, R. and Hansen, L.A. (1991) Cortical and subcortical patterns of synaptophysin-like immunoreactivity in Alzheimer's disease. *Am. J. Pathol.*, **138**, 235–246.
73. Terry, R.D., Masliah, E., Salmon, D.P., Butters, N., DeTeresa, R., Hill, R., Hansen, L.A. and Katzman, R. (1991) Physical basis of cognitive alterations in Alzheimer's disease: synapse loss is the major correlate of cognitive impairment. *Ann. Neurol.*, **30**, 572–580.
74. DeKosky, S.T. and Scheff, S.W. (1990) Synapse loss in frontal cortex biopsies in Alzheimer's disease: correlation with cognitive severity. *Ann. Neurol.*, **27**, 457–464.
75. Falzone, T.L., Stokin, G.B., Lillo, C., Rodrigues, E.M., Westerman, E.L., Williams, D.S. and Goldstein, L.S. (2009) Axonal stress kinase activation and tau misbehavior induced by kinesin-1 transport defects. *J. Neurosci.*, **29**, 5758–5767.
76. Chen, X.H., Siman, R., Iwata, A., Meaney, D.F., Trojanowski, J.Q. and Smith, D.H. (2004) Long-term accumulation of amyloid-beta, beta-secretase, presenilin-1, and caspase-3 in damaged axons following brain trauma. *Am. J. Pathol.*, **165**, 357–371.
77. Smith, D.H., Chen, X.H., Iwata, A. and Graham, D.I. (2003) Amyloid beta accumulation in axons after traumatic brain injury in humans. *J. Neurosurg.*, **98**, 1072–1077.
78. Iwata, A., Chen, X.H., McIntosh, T.K., Browne, K.D. and Smith, D.H. (2002) Long-term accumulation of amyloid-beta in axons following brain trauma without persistent upregulation of amyloid precursor protein genes. *J. Neuropathol. Exp. Neurol.*, **61**, 1056–1068.
79. Stone, J.R., Okonkwo, D.O., Singleton, R.H., Mutlu, L.K., Helm, G.A. and Povlishock, J.T. (2002) Caspase-3-mediated cleavage of amyloid precursor protein and formation of amyloid beta peptide in traumatic axonal injury. *J. Neurotrauma*, **19**, 601–614.
80. Kawarabayashi, T., Shoji, M., Yamaguchi, H., Tanaka, M., Harigaya, Y., Ishiguro, K. and Hirai, S. (1993) Amyloid beta protein precursor accumulates in swollen neurites throughout rat brain with aging. *Neurosci. Lett.*, **153**, 73–76.
81. Falzone, T.L., Gunawardena, S., McCleary, D., Reis, G.F. and Goldstein, L.S. (2010) Kinesin-1 transport reductions enhance human tau hyperphosphorylation, aggregation and neurodegeneration in animal models of tauopathies. *Hum. Mol. Genet.*, **19**, 4399–4408.
82. Stamer, K., Vogel, R., Thies, E., Mandelkow, E. and Mandelkow, E.M. (2002) Tau blocks traffic of organelles, neurofilaments, and APP vesicles in neurons and enhances oxidative stress. *J. Cell Biol.*, **156**, 1051–1063.
83. Ebneth, A., Godemann, R., Stamer, K., Illenberger, S., Trinczek, B. and Mandelkow, E. (1998) Overexpression of tau protein inhibits kinesin-dependent trafficking of vesicles, mitochondria, and endoplasmic reticulum: implications for Alzheimer's disease. *J. Cell Biol.*, **143**, 777–794.
84. Kaether, C., Skehel, P., Dotti, C.G. and Haass, C. (2006) Axonal membrane proteins are transported in distinct carriers: a two-color video microscopy study in cultured hippocampal neurons. *Mol. Biol. Cell*, **11**, 1213–1224.
85. Kaether, C., Schmitt, S., Willem, M. and Haass, C. (2006) Amyloid precursor protein and Notch intracellular domains are generated after transport of their precursors to the cell surface. *Traffic*, **7**, 408–415.